Advances in Water Resources 37 (2012) 94–103

Contents lists available at SciVerse ScienceDirect

Advances in Water Resources

journal homepage: www.elsevier.com/locate/advwatres

Multiple mechanisms generate Lorentzian and $1/f^{\alpha}$ power spectra in daily stream-flow time series

Sally E. Thompson [a,b,*], Gabriel G. Katul [a,c]

[a] Nicholas School of the Environment, Duke University, Durham, North Carolina, USA
[b] Department of Civil and Environmental Engineering, University of California, Berkeley, California, USA
[c] Pratt School of Engineering, Duke University, Durham, North Carolina, USA

ARTICLE INFO

Article history:
Received 7 June 2011
Received in revised form 12 October 2011
Accepted 28 October 2011
Available online 25 November 2011

Keywords:
Fourier spectrum
Power-law
Power spectra
Streamflow
Unit hydrograph
Water balance

ABSTRACT

Power-law scaling is an ubiquitous feature of the power spectrum of streamflow on the daily to monthly timescales where the spectrum is most strongly affected by hydrologic catchment-scale processes. Numerous mechanistic explanations for the emergence of this power-law scaling have been proposed. This study employs empirical spectra obtained for eight river basins in the South Eastern US and synthetic spectra generated from a range of proposed mechanisms to explore these explanations. The empirical analysis suggested that streamflow spectra were characterized by multiple power-law scaling regimes with high-frequency exponents α in the range -1 to -5. In the studied basins, α tended to increase with drainage area. The power-law generating mechanisms analyzed included linear and non-linear catchment water balance arguments, power-law recession behavior, autonomous and non-autonomous responses of channel hydraulics and the n-fold convolution of linear reservoirs underpinning Dooge or Nash hydrographs. Of these mechanisms, only n-fold convolutions with $n = 2$ or 3 generated power spectra with features that were consistent with the empirical cases. If the effects of daily streamflow sampling on truncating power spectra were considered, then the trends in α with drainage area were also consistent with this mechanism. Generalizing the linear convolution approach to a network of reservoirs with randomly distributed parameters preserved the features of the power spectrum and maintained consistency with empirical spectra.

1. Introduction

1.1. Streamflow signatures

Streamflow provides an integrated measure of up-gradient hydrological processes within a catchment, making it a key metric to characterize the behavior of natural systems [1]. Analysis of streamflow timeseries has multiple hydrologic applications, from estimating evapotranspiration and precipitation history [2–4], making inferences about hillslope travel time distributions [5,6], antecedent water content [7], channel-aquifer connections [8,9] and analyzing baseflow generation processes [10].

Streamflow measurements can be interpreted in several ways, perhaps most widely through direct analysis of the flow hydrograph, for example in hydrograph recession analysis [10]. Alternatively, streamflow can be analyzed in a probabilistic framework, for instance by determining the nature and controls on the probability density function (pdf) of streamflow. Such probabilistic analyses provide insight into the 'filtering' of the stochastic rainfall signal by the landscape [11,12], and allow risk and likelihood-based interpretations of streamflow variability. Probabilistic analyses describe only the variations in the magnitude of runoff, however, and are therefore complemented by information that characterizes the temporal structure of these variations, for example through the correlation structure or power spectrum of the timeseries. These approaches emphasize periodicities and persistence and enable contributions of different processes to the total streamflow variability to be separated on the basis of their characteristic timescales. Spectral interpretations of flow variability are receiving increasing interest [13–17] due to the information they reveal about clustering, intermittency and long-term memory in hydrological systems. Numerous mechanistic explanations have been proposed to explain the widely observed features of streamflow power spectra. This study compares the synthetic spectra generated by multiple mechanisms to empirically derived spectra obtained for eight river basins in the South Eastern US, and evaluates the ability of the mechanistic explanations to reproduce key features of the empirical spectra, and in particular the scaling exponents.

* Corresponding author at: Nicholas School of the Environment, Duke University, Durham, North Carolina, USA.
E-mail address: set8@duke.edu (S.E. Thompson).

0309-1708/$ - see front matter © 2011 Elsevier Ltd. All rights reserved.
doi:10.1016/j.advwatres.2011.10.010

1.2. The streamflow power spectrum

The streamflow power spectrum is defined by the Fourier transform of the streamflow timeseries $q(t)$:

$$Q(f) = \int_{-\infty}^{\infty} q(t)\exp(\mathbf{i}ft)dt, \quad (1)$$

where $\mathbf{i}^2 = -1$, $f[T^{-1}]$ is a frequency coordinate and $t[T]$ is the time coordinate. The energy spectrum is given by the squared amplitude of the transformed flow, $|Q(f)|^2 df$. The power spectrum is defined by the energy per unit frequency $|Q(f)|^2$. The power spectrum is related to the variance of the original timeseries σ^2, by Parseval's theorem: $\sigma^2 = 2\int_{f=0}^{\infty} Q(f)df$. The power spectrum is defined on an infinite domain of frequencies, and different processes inject energy at different timescales, as illustrated in Fig. 1. In the case of streamflow, the high frequency component of the spectrum (timescales on the order of seconds) is dominated by the action and the spectral signature of turbulence (for large Reynolds number flow). At low frequencies (seasonal to –inter-annual timescales), streamflow spectra most strongly reflect climatic drivers. The influence of the landscape and hydrological processes is most pronounced at approximately daily timescales, and the focus here is therefore on the timescales bounding the 'hydrologic regime' shown in Fig. 1. The power spectrum of streamflow at these timescales is closely related to the instantaneous unit hydrograph (IUH) of the watershed [18] denoted as $u(t)$. By construction,

$$q(t) = \int_0^t (p(\tau) - l(\tau))u(t-\tau)d\tau, \quad (2)$$

where $p(t)$ is the hyetograph, and $l(t)$ is a loss function accounting for the differences in mass between rainfall and streamflow. Denote the difference of p and l as p_q, defining the volume of rainfall input to the catchment that is potentially available for flow generation. The properties of the Fourier convolution integral require that:

$$Q(f) = P_Q(f) \times U(f), \quad (3)$$

where $P_Q(f)$ and $U(f)$ are the Fourier transforms of p_q and the IUH, respectively. Thus, the streamflow power spectrum normalized by the power spectrum of p_q defines the power spectrum of the IUH. The IUH can be interpreted as a linear 'transfer function' translating rainfall spectral forcing into streamflow spectral response within the timescales of the hydrologic regime in Fig. 1. On timescales where p_q can be approximated as white noise, the power spectrum of streamflow will closely reflect the power spectrum of the IUH. Because the Fourier transform acts as an ensemble averaging operator, this view of the IUH depicts the mean catchment response to rainfall, and cannot be used to interpret or make predictions about the watershed response to individual rainfall events. Any non-stationarity in these responses is averaged out in both the IUH and the spectrum, and any further modification of the rainfall signature – for instance by travel through the vadose zone – is incorporated as part of the IUH.

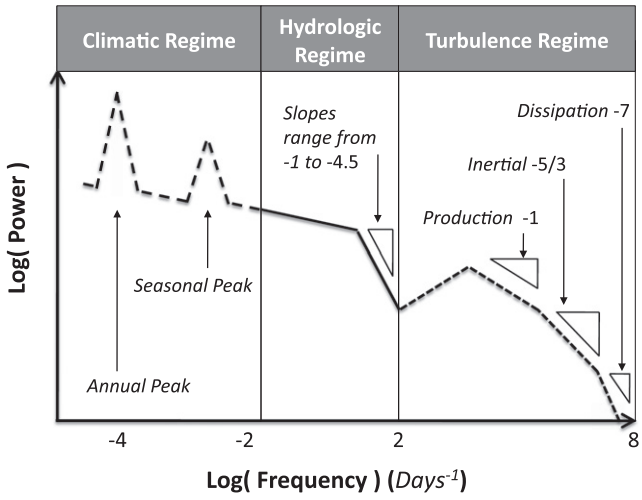

Fig. 1. Conceptual diagram of the full power spectrum of streamflow. At high frequencies (corresponding to fluctuations on the order of seconds) the Kolmogorov Turbulent cascade emerges in the spectrum, characterized by the −5/3 power law scaling in the inertial regime, steeper scaling in the dissipative region and −1 scaling in the production region. At the lowest frequencies periodic features associated with seasonal, annual and longer period cycles emerge in the spectrum, primarily associated with climatic drivers of streamflow. The intermediate regime in the scaling range of hours to months is associated with fluctuations that are hydrologically mediated, that reflect the nature of the instantaneous unit hydrograph, and which are the focus of this study.

1.3. Characteristics of the streamflow power spectrum

Daily USGS streamflow records from eight river basins in North Carolina were analyzed to illustrate some features of the streamflow power spectrum. North Carolina has a warm humid climate with persistent, rain-driven streamflow, making it an appropriate location to investigate streamflow dynamics year-round. Gages with a minimum record of 20 years were used here. Up to 115 years of flow data were available in some locations, and the mean record length in the dataset was 60 years. Gages were selected along the main river stems. Because most rivers on the eastern seaboard of the USA have been subject to dam construction, streamflow gages located upstream of major control structures were selected whenever possible (Lumber River, Rappahannock River, French Broad River, New River): the effect of dams on the spectra in the other basins is discussed below. The gages are for drainage areas ranging from 38 km^2 to nearly 22,000 km^2. Metadata regarding the gages used are provided in Table 1.

Several methods were applied to remove the effects of slow variations in the streamflow prior to analysis. These included a high-pass wavelet filter, and a two-parameter Chapman recursive digital filter for baseflow separation [19,20]. The Chapman filter has been shown to perform comparably to other baseflow separation algorithms [21], and the different approaches had little overall influence on the resulting spectra. Troch et al. [22] found that water balance metrics were also relatively insensitive to the choice of baseflow separation algorithm. The Chapman filter was retained, and the resulting timeseries of direct runoff was normalized to have a mean of zero and standard deviation of unity (m^3/day). Fourier transforms of the resulting timeseries were conducted using the Fast Fourier Transform algorithm, and power spectra generated from the squared Fourier amplitudes. The resulting power spectra were characterized by near-linear scaling regimes with a 'break' in the scaling evident at timescales on the order of 5–10 days. Power spectra of this nature are special forms of the Von Karman spectrum:

$$|Q(f)|^2 \propto \frac{1}{\left(\omega_x^2 + f^\alpha\right)^n} \quad (4)$$

and with $n = 1$ and $\alpha = 2$, these spectra recover a Lorentzian functional form. A true Lorentzian function converges on white noise at sufficiently small f. The low-frequency spectra of streamflow, however, retained features of power-law scaling. To isolate the effect of reddening at high frequencies, the approach of Dolgonosov et al. [17] was used, and the function:

$$|Q(f)|^2 \propto \frac{1}{f^\zeta}\frac{1}{\omega_x^2 + f^\alpha}, \quad (5)$$

was fitted to the empirical power spectra for frequencies in the range $0.01 < f < 1$ day^{-1}. Noise in the power spectrum can confound

Table 1
North Carolina river basin data including dates of dam installation and comparisons of power spectral exponents pre-dam construction and for the full record.

Basin	Locality	Drainage area (km^2)	Elevation (m a.s.l.)	Duration	Control structures	α Full record	α Pre-dam	% Change
Tar River, NC	Tar River	433	286	1939–1984	Rocky Mount Reservoir	2.01	2.00	0.5
	Louisberg	1106	176	1963–2008	completed 1971	2.21		
	Nashville	1816	111	1928–1970		2.94	2.94	0.0
	Rocky Mount	2396	53	1976–2010		3.27		
	Tarrboro	5654	9	1896–1941		4.10	4.20	2.5
Rappahannock, VA	Warrenton	505	312	1942–1986	River dammed below	2.08		
	Remington	1603	253	1942–1987	Fredricksberg.	3.60		
	Kellys Ford	1660	208	1927–1952	Removed 2004	3.59		
	Fredericksberg	4131	70	1907–1952		3.36		
Deep River, NC	High Point	38	764	1928–1973	12 Dams along the	0.44		
	Randleman	324	640	1928–1973	course of the river	1.38		
	Ramseur	904	420	1923–1968	including 3 large lock	1.88		
	Moncure	3714	185	1930–1975	structures at the river	2.31		
	Lillington	8972	105	1924–2010	mouth	2.58		
	Wilmington	12567	30	1937–2010		2.40		
	Kelly	13610	0	1969–2010		3.89		
Neuse River, NC	Northside	1386	226	1927–1980	Falls Lake Dam	3.68	3.68	0.0
	Clayton	2978	128	1927–2010	completed 1981	2.88	2.88	0.0
	Smithfield	3124	100	1970–1991		2.99		
	Goldsboro	6213	43	1930–2010		3.56	4.19	15
	Kinston	6946	11	1930–2010		3.94	3.87	1.9
Roanoke River, NC & VA	Roanoke	995	906	1899–2010	Kerr Lake completed	1.63	2.41	32.5
	Niagara	1318	820		1952 other dams	3.70	3.71	0.2
	Toshes	2634	588	1925–1963	constructed later	2.81	2.79	0.6
	Altavista	4615	503	1930–2010		3.63	3.63	0
	Brookneal	6226	351	1923–2010		3.89	3.89	0.0
	Randolph	7682	307	1901–2010		4.49	4.49	0
	Clover	8358	302	1929–1952		3.56		
	Rnke. Rapids	21714	44	1912–2010		3.70	3.70	0.0
French Broad, NC	Rosman	176	2174	1907–2010	Impounded at Douglas	3.24		
	Blantyre	767	2060	1920–2010	Dam, downstream of	3.08		
	Bent Creek	1751	1996	1934–1986	Marshall	3.18		
	Asheville	2448	1950	1895–2010		3.25		
	Marshall	3450	1646	1942–2010		3.61		
Lumber River, NC	Maxton	945	171	1987–2010	Uncontrolled	1.06		
	Boardman	3181	72	1929–2010		2.86		
New River NC & VA	Jefferson	531	2657	1924–2010	Impounded	1.34		
	Galax	2955	2208	1929–2010	downstream of	2.84		
	Ivanhoe	3496	1943	1927–2010	Allistonia	2.89		
	Allistonia	5729	1848	1929–2010		3.23		

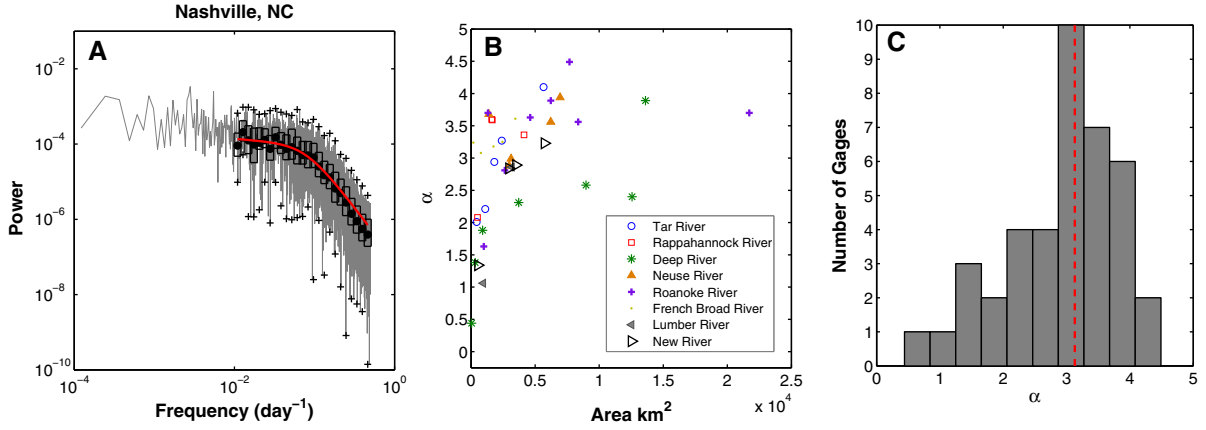

Fig. 2. Analysis of streamflow spectra from North Carolina Rivers. Panel (A) shows a raw spectrum for Nashville NC. Superimposed on the spectrum are 25 logarithmic bins. The mean value of the bins is shown as a dark spot, boxes indicate the interquartile range, and crosses the minima and maxima within each bin. The fit of Eq. (5) for this basin is indicated in red. Panel (B) illustrates the general increasing trend in the computed high-frequency exponent with increasing basin size for each of the 40 gages studied. Panel (C) illustrates the relatively constrained values of the scaling exponent α, ranging from approximately 0.5 to 4.5, with a median of 3.5. (For interpretation of the references to colour in this figure legend, the reader is referred to the web version of this article.)

Table 2
Features of streamflow power spectral scaling reported in other studies. Note that the highest value of α was obtained by the study using the highest sampling frequency.

Study	Basin scale km^2	Sample freq.	α	A
Schilling and Zhang [43]	52.18	Hourly	3.65	19 h
Dolgonosov et al. [17]	1850–21,000	Daily	2–3.0	12 days
Pandey et al. [14]	5–1.8 $\times$ 10^6	Daily	2.75 (mean)	1 week
Tessier et al. [47]	40–200	Daily	1–2.1	16 days

fitting, so the spectra were smoothed using a logarithmic binning approach. In this approach, the data are binned by frequency such that the log of the bin width is constant, thus avoiding biasing the fit towards higher frequencies [23]. The mean value in each bin is then computed and used to fit the Lorentzian to the spectrum, as illustrated in Fig. 2. The values of α obtained from the fitting are shown in Table 1.

The spectra had two other important features. Firstly, the range of α values was relatively constrained. As illustrated in Fig. 2, the exponents obtained empirically ranged from 0.5 to 4.5, with median values of 3.5. Secondly, within each basin (and overall) there was an increasing trend in α with drainage area, also shown in Fig. 2.

In four basins data from gages located downstream of dams were included. The dates of dam installation range from the 1800s (Deep River), 1952 (Roanaoke River), 1971 (Tar River) to 1981 (Neuse River). With the exception of the Deep River, there are long enough streamflow records in these rivers to allow the effects of dam construction on the streamflow spectra to be evaluated. As shown in Table 1, of the thirteen gages for which spectra were compared before and after dam construction (gages where there were at least 20 years of "pre-dam" data), only two showed alterations of more than 5% in the α exponent. On this basis we maintained the full flow records for the basins. The early installation of locks in the Deep River means that the alteration of the natural regime induced by the dams could not be independently evaluated.

The features of the streamflow spectrum identified for the North Carolina rivers are consistent with other studies, summarized in Table 2. These studies also identified multiple scaling regimes in the streamflow spectra and obtained α values on the order of -2 to -3.75 (for references, see Table 2). These estimates of α were made on timescales ranging from less than a day to approximately 2 weeks, that is within the hydrologic regime of Fig. 1.

2. Mechanisms generating power-law responses in spectra

The potential mechanisms that could result in power-law responses in streamflow spectra at daily–monthly time scales are now reviewed, and their features compared to the empirical streamflow spectra. The mechanisms are divided into two broad categories: purely deterministic phenomena that could lead to power-law spectra when forced by random rainfall, and phenomena in which random spatial heterogeneity is explicitly considered along with the random rainfall forcing.

2.1. Deterministic processes

2.1.1. Note on terminology

Analytical manipulation via Fourier transforms is generally only possible for linear processes. These analyses therefore rely on linear representations of flow generation, such as: $q(t) = q_o \exp(-kt)$. The constant k has units of T^{-1}. Although it is natural to interpret k as a residence time, this interpretation does not reflect current understanding of runoff generation processes in most catchments (e.g. the old water paradox [24,25]). Tracer experiments indicate that residence times within the vadose and saturated zones can be long, while k typically has timescales of days to weeks. Hence k should be interpreted as the timescale on which rainfall events generate runoff responses. Mechanistically, k may be related to the persistence of pressure connectivity between saturated regions in the hillslope with the riparian zone. For clarity, k is referred to as the "response timescale" of the linear reservoir.

2.1.2. Linear water balance

One approach to deriving the streamflow spectrum begins by expressing stream discharge as a function of catchment water balance [2,16,17]:

$$et(t) = p(t) - \frac{1}{A}\left(q(t) + \frac{ds}{dt}\right), \tag{6}$$

where et is evapotranspiration, p is precipitation, A is the contributing drainage area, s is the volume of water stored in the catchment and t indicates time. Assuming a power-law storage-discharge relation: $q = as^b$, where a and b are catchment-specific parameters, discharge can be isolated:

$$-q^{(b-1)/b} a^{1/b} b(A\, et(t) - A\, p(t) + q(t)) = \frac{dq}{dt}. \tag{7}$$

The Fourier transform of Eq. (7) can be analytically determined if $(b-1)/b \sim 0$ (or $b \sim 1$, a linear storage-discharge relationship), giving:

$$Q(f) = \frac{\gamma(\beta + \mathbf{i}f)(P(f) - E(f))}{(\beta^2 + f^2)}, \tag{8}$$

where $\beta = a^{1/b} b$ and $\gamma = \beta A$, and where P, E and Q are the Fourier transforms of p, et and q, respectively. Computing the power spectrum of the streamflow gives:

$$|Q(f)|^2 = \frac{\gamma^2(|P(f) - E(f)|^2)}{(\beta^2 + f^2)}. \tag{9}$$

Fluctuations in et at daily and longer timescales are likely to have a smaller amplitude than fluctuations in p [26] within the hydrologic regime (Fig. 1), and so it might be reasonable to assume that:

$$|P(f) - E(f)|^2 \approx |P(f)|^2, \tag{10}$$

for daily–monthly frequencies. At higher and lower frequencies, the diurnal cycle in et, within-storm temporal scaling and seasonal variations in p and et invalidate this approximation. To illustrate, p and et scaling were examined from eddy-covariance and rainfall timeseries collected at the Duke Forest's Blackwood division near Durham NC. Eight years of data gathered in a pine plantation, and five years of data gathered in a hardwood forest and grass field [27,28] were analyzed. As shown in Fig. 3, Eq. (10) was a good approximation on daily to monthly timescales for all three ecosystems, but broke down for $f < 0.01$ or $f > 1$ days^{-1}. With Eqs. (10), (9) simplifies to a Lorentzian form for $|Q(f)|^2/|P(f)|^2$, with:

$$\frac{|Q(f)|^2}{|P(f)|^2} \propto \frac{1}{(\beta^2 + f^2)}, \tag{11}$$

so that at high f, $|Q(f)|^2 \sim f^{-2}$. By comparing Eqs. (11) and (4), it is inferred that the catchment water balance constrains the streamflow spectrum to a Lorentzian form. However, it is apparent that this form of scaling cannot result in power-law exponents that deviate from -2. Plausibly, the deviations in α from -2 might derive from nonlinear storage discharge relationships, where $q = as^b$ but b is no longer constrained by $(b-1)/b \sim 0$. Such nonlinear relationships often

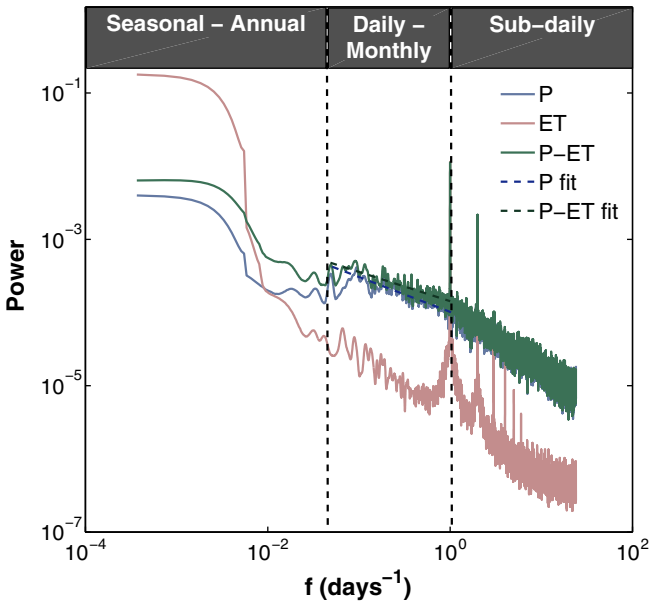

Fig. 3. Comparison of the power spectra of precipitation, evapotranspiration and their difference from timescales ranging from daily to inter-annual for 8 years of data collected at a pine plantation in North Carolina. Linear trends from the 100 daily to daily timescales are shown for comparison. It is evident that at monthly to daily timescales, there is very little difference in the spectra of P and of $P - ET$, in part due to the relatively low variance in ET at those timescales. Similar trends were found over 5 years of data for a broadleaf forest and grass field.

arise in real situations [29]: for instance, solutions of the Boussinesq Equation for an unconfined, homogeneous horizontal aquifer suggest that $b \in [1.5–3]$ [2]; Palmroth et al. [3] found that $b \in [1.1–1.6]$ for a series of North Carolina watersheds, while Ceola et al. [30] found $b \in [1,2.2]$. Furthermore, Biswal and Marani [31] suggested that the parameters a and b could be related to network geomorphology, resulting in spatially-dependent and nonlinear storage-discharge relationships.

2.1.3. Nonlinear water balance

No analytical treatment of the Fourier transform of Eq. (7) is possible when $b \neq 1$. However, the sensitivity of $|Q(f)|^2$ to varying b can be explored by solving Eq. (7) numerically. Numerical solutions to Eq. (7) obtained using Milstein's Higher Order Method [32] assuming white noise for $P(t) - E(t)$ are shown in Fig. 4. The solutions shown are ensemble means of 100 simulations generated for b in the range 1 through 5 and normalized to zero mean and unit variance. Although the break in scaling and the intercepts of the spectra shift with b, the slopes of the spectra at higher frequencies remain unchanged at ≈ 2. The non-linearity in the storage-discharge therefore does not explain the $\alpha \neq 2$. This result is consistent with analyses of the higher-order power spectra of fluid turbulence, where the "higher-order power spectrum" refers to the power spectrum of a quantity raised to a power m, when $m > 1$. The higher order spectra of fluid turbulence preserves Kolmogorov's $-5/3$ scaling (i.e. the expected scaling at high frequencies for high Reynolds Number turbulent flows) for all m, a result that can be shown arise for any timeseries with near-Gaussian fluctuations [33,34]. Thus, including the nonlinearity in Eq. (7) does not alter the spectral scaling from the linear case. The water balance approach cannot therefore explain the full range of $1/f^{\alpha}$ slopes observed in streamflow power spectra (Fig. 2).

2.1.4. Power-laws in the recession drive power-laws in the spectrum

Power-law behavior in hydrograph recessions is widely observed. The hydraulics of porous media flow draining from the hillslope are often invoked as drivers of power-law behavior in the hydrograph recession [2,35]. Alternative explanations that rely primarily on heterogeneity of travel times across multiple flow paths also predict power-law recession behavior [5,6,31]. Power-law behavior in hydrograph recessions implies that during the recession phase, $q \propto t^{-\omega}$. The Fourier transforms of such recessions cannot be analytically determined in general. Heuristically, the more negative ω is, the more the IUH resembles an impulse function, and the less the incoming signal of rainfall is 'reddened' during the recession phase. Conversely, the closer ω is to zero, the greater the attenuation and reddening of the input signals. For $0 < \omega < 1$ the Fourier power spectrum of $q \propto t^{-\omega}$ can be analytically determined and is given by:

$$|Q(t)|^2 = 4(f^2)^{\omega-1}\Gamma(1-\omega)^2 \sin(\pi\omega)^2. \quad (12)$$

Evidently, as $\omega \to 1$ less reddening of the spectrum can be attributed to the recession, while as $\omega \to 0$ the spectral scaling approaches $1/f^2$. Therefore, power law recessions produce scaling behavior bounded by $0 < \alpha < 2$, which is too restrictive to explain the range of observed empirical behavior.

2.1.5. Series of linear reservoirs drive power-laws in the spectrum

If the streamflow spectrum is approached from the perspective of the instantaneous unit hydrograph, then the unit hydrograph

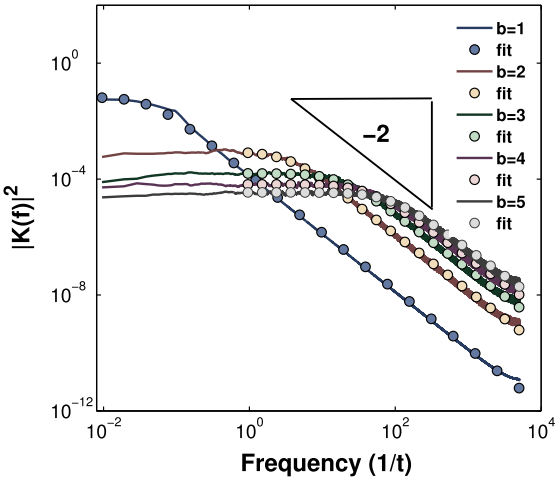

b	A	B	α
1	0.012	0.045	2.0
2	0.097	3.3	1.9
3	0.20	16	1.9
4	0.25	31	1.8
5	0.35	59	1.8

Fig. 4. Ensemble mean power spectra generated for nonlinear analogues to Eq. (7). Fits of the Lorentzian (represented as $A/(B^2 + f^{\alpha})$) are shown in the table for each value of the storage-discharge exponent (b). A -2 grade line is shown for reference.

models of Dooge [36] and Nash [37] provide an alternative explanation for the spectral phenomena. These models conceptualize hydrographs as arising from the successive transformation of a flood peak by travel through n linear reservoirs or channels. In each case, the unit hydrograph can be defined as a gamma distribution of the form:

$$u(t) = \frac{1}{k\Gamma(n)}\left(\frac{t}{k}\right)^{(n-1)} \times \exp\left(\frac{-t}{k}\right), \quad \text{(linear reservoirs)}, \tag{13}$$

$$u(t) = \frac{1}{k\Gamma(n)}\left(\frac{t-nT_C}{k}\right)^{(n-1)} \times \exp\left(\frac{-(t-nT_C)}{k}\right), \quad \text{(linear channels)}, \tag{14}$$

where k is interpreted as the reservoir response timescale as before, and T_C represents the travel time in the channels. These unit hydrographs have identical power spectra:

$$|U(f)|^2 = (\Gamma(n))^2 \frac{1}{(1/k^2 + f^2)^n}. \tag{15}$$

When $n = 1$, this result is identical to that in Eq. (11). These unit hydrographs thus generalize the water balance approach by propagating it through n reservoirs in series, permitting multiple scaling regimes with $\approx 1/f^{2n}$. Encouragingly, this conceptual model permits $\alpha > 2$. Given the constrained range of α values observed in the daily–monthly regime, however, this model suggests that river basins consist of at most 2–3 linear stores in series. While $n \sim 3$ does not map logically to a discretization of reservoirs based on, for instance channel order or drainage area, it may be appropriate if catchments are conceptualized as consisting of a small number of different 'kinds' of reservoirs, distributed in space and connected through a network structure. These reservoirs could feasibly consist of the vadose zone, shallow responsive saturated zones, and the channel network itself. The generalization of this conceptual model to a primitive form of such a network is addressed in Section 2.2.

2.1.6. Channel hydraulics generate power-law responses in the spectra

Here we explore two novel hypotheses for the genesis of streamflow power-laws: autonomous and non-autonomous responses of the channel. The first hypothesis is that the autonomous response of streamflow hydraulics to lateral inputs of flow can generate power-laws in the streamflow spectrum. The starting point is the kinematic version of the shallow water continuity equation [38]:

$$\frac{\partial h}{\partial t} + \frac{\partial (Vh)}{\partial x} = q_L, \tag{16}$$

where h is the stage in the channel, V the velocity, x the longitudinal coordinate, and q_L represents the lateral input to the channel per unit width of channel (units L/T). If a kinematic relationship between stage and velocity of the form $V = K_r h^v$ is assumed, then the continuity equation can be expanded as:

$$\frac{\partial h}{\partial t} + K_r(1+v)h^v \frac{\partial h}{\partial x} = q_L. \tag{17}$$

For locally uniform flow the water depth gradient can be approximated as a constant, equivalent to the bed slope S_o, giving:

$$\frac{\partial h}{\partial t} + S_o K_r (1+v) h^v = q_L \tag{18}$$

and the solution to the homogeneous (autonomous) equation where $q_L = 0$ (i.e. when water arrives in the stream as a Dirac delta pulse) can be found as:

$$h = (v-1)(S_o K_r t(v+1) - c_1)^{1/(1-v)}. \tag{19}$$

The constant c_1 can be estimated from the stage prior to the beginning of the runoff event, h_0, as $c_1 = h_0^{1-v}/(1-v)$. Provided that h_0 is small, $c_1 \sim 0$. From dimensional analysis, $q \approx h\frac{\partial h}{\partial t}$, so that the flow $q(t)$ associated with the autonomous response can be estimated as:

$$q(t) \approx -S_o K_r (1+v)((v-1)(S_o K_r t(1+v)))^{\frac{1+v}{1-v}}. \tag{20}$$

The rate of change of the flow is then estimated as:

$$\frac{dq}{dt} = -\frac{q(1+v)}{t(v-1)} \approx \frac{q}{t}\left(1 - \frac{\lambda}{2}\right). \tag{21}$$

If this flow component represents the rising limb of the hydrograph, and recessions are assumed to be near exponential, then the ordinary differential equation (ODE) describing the evolution of the runoff hydrograph can be expressed as the superposition of rising and falling components:

$$\frac{dq}{dt} = \frac{q}{t}\left(1 - \frac{\lambda}{2}\right) - \omega_x q, \tag{22}$$

where ω_x is the response timescale of the channel. Solving for the time evolution of the flow yields:

$$q(t) = t^{\frac{\lambda}{2}-1}\exp(-\omega_x t). \tag{23}$$

The hydraulic argument recovers the canonical gamma distribution form of the unit hydrograph as per Section 2.1.5, but with a rather different mechanistic underpinning. Power spectra generated from this relationship scale as $1/f^2$, suggesting that the autonomous hydraulic response of the rising limb of the flood hydrograph is consistent with the production of power spectra with $\alpha > 2$. Although initially encouraging, closer inspection of this derivation suggests that it is subject to a significant caveat. Solving the substitution made in Eq. (21) for λ:

$$\lambda = 4v/(v-1). \tag{24}$$

This relationship has an asymptotic minimum for λ of 4 as $v \to \infty$, and predicts $\lambda < 0$ for typical values of v (such as $v \sim 2/3$ from Manning's Equation).

An alternative hypothesis is that the non-autonomous component of the hydraulic response could drive power-laws in the spectrum. During the rising phase of the hydrograph, it is reasonable to assume that the non-local input of water to the channel is the dominant term, so that the continuity equation may be reduced to:

$$\frac{\partial h}{\partial t} \approx q_L \propto \frac{h}{t}, \tag{25}$$

where a scaling argument has again been applied to approximate q_L. Applying the kinematic relationship, $V = K_r h^v$ this can be re-expressed in terms of the flow:

$$\frac{\partial q}{\partial t} = \xi \frac{q}{t}(v+1), \tag{26}$$

where ξ is a constant of proportionality. This simple scaling argument recovers the solution for the rising limb of a runoff hydrograph driven by steady rainfall and shallow kinematic flow [38]. Assuming an exponential recession, the hydrograph ODE is:

$$\frac{dq}{dt} = \xi \frac{q}{t}(v+1) - \omega_x q, \tag{27}$$

with solution $q = \exp(-\omega_x t)t^{\xi(1+v)}$. This solution generates $1/f^\alpha$ scaling with $\alpha = 2(1 + \xi + \xi v)$. Assuming $v \approx 2/3$, exponents in the range of 2 to 5 are recovered for $0.3 < \xi < 1$. To determine if these values are reasonable in light of measured hydrographs, individual flood events were isolated from the NC river data and the relationship $\frac{dq}{dt} = \theta\frac{q}{t}$ fitted to the rising limbs. The values of θ obtained ranged from 2.6 to 11.5, giving ξ in the range 1.6 to 6.85, and α of 7 to 25, much greater than observed empirically. Perhaps the prediction

of large values of the spectral exponent is unsurprising given the non-stationarity within the non-autonomous term, which would be expected to generate strong coherence and memory effects for the individual flood events analyzed.

The hydraulic hypotheses provide an alternative way to conceptualize the genesis of the unit hydrograph based on channel flow alone. They provide a flexible interpretation of multiple values of power spectral scaling, and the emphasis on the rising limb as generating power-laws in the spectrum appears to be appropriate. Furthermore, the hypothesized power-law rise was found to be a reasonable description of the rising limb of the streamflow hydrograph. The lack of a quantitative agreement between these predictions and observation may therefore indicate alternative derivations of a $dq/dt \sim q/t$ relationship for the rising limb are needed to reconcile the high values of θ with the observed values of α. Alternatively, the fact that rising limb fits can only be computed for isolated storms may result in a bias in the estimation of θ by comparison to the full flow record, generating the quantitative mismatch.

2.2. Stochastic approach

Having reviewed a range of deterministic hypotheses for the generation of power-law scaling in the streamflow spectrum, the conceptual model that appears to be most consistent with observations is that of 1–3 reservoirs in series. This conceptualization can be generalized to real catchments by assuming these reservoirs are arranged in a spatially distributed network. As a starting point, each reservoir is assumed to act as a linear reservoir with a distinct response timescale, $k_{i,j}$ where i indicates the order of the reservoir – i.e. its location along a single flow path of reservoirs in series – and j denotes the specific individual reservoir. The components of the network are reservoirs in series (connecting reservoirs of different order i) and reservoirs in parallel (describing the behavior of multiple individual reservoirs j at the same order i), as illustrated conceptually in Fig. 5. These components are first investigated in isolation from each other.

2.3. Reservoirs in parallel with random time constants

Let each reservoir j be characterized by a single time constant k_j. Then the discharge from an individual reservoir has the form:

$$q_j(t) = q_{oj}\exp(-k_j t). \tag{28}$$

Assume that the values of k are randomly distributed across the parallel reservoirs (due to heterogeneity in subcatchment area, soils, geology, etc. [31]) according to a known probability density function $p_k(k)$. Using the combined distribution approach [39,40], the resulting discharge $q_n(t)$ from the set of n parallel reservoirs (assuming each reservoir contributes an equivalent volume) can be estimated as:

$$q_n(t) = \int_0^\infty q_o \exp(-kt)\; p_k(k)\mathrm{d}k. \tag{29}$$

For many choices of $p_k(k)$ Eq. (29) generates analytical solutions that are simple power-laws in time, as shown in Table 3. Based on the recession analysis discussed in Section 2.1.4, the power spectra of these recessions would be expected to have $0 < \alpha < 2$. The power spectra of the functions shown in Table 3 were computed while varying their parameters over 9 orders of magnitude (from 10^{-4} to 10^{4}). The results are shown in Table 3 and confirm that the power spectra exponents remained in the range 0 to −2. Furthermore, visual inspection of the spectra indicated that deviations from $1/f^2$ scaling only occurred when the spectra were truncated at higher frequencies. These results suggest that discharge relationships derived from parallel combinations of linear reservoirs preserve $1/f^2$ scaling in the spectra.

2.4. Reservoirs in series with random time constants

The other structural element of a network of reservoirs are chains of reservoirs in series with randomized time constants. The Fourier transform of the individual reservoir considered in Eq. (28) is:

$$Q(f)_j = \frac{q_{oj}}{k_j + \mathbf{i}f}. \tag{30}$$

In the Fourier Domain, the n-fold convolution of the exponential reservoir can be readily computed:

$$Q(f)_n = \prod_{j=1}^{n}\frac{q_{oj}}{k_j+\mathbf{i}f} = \prod_{j=1}^{n} q_{oj}\prod_{j=1}^{n}\frac{1}{(k_j+\mathbf{i}f)}, \tag{31}$$

which leads to a power spectrum:

Table 3
Generation of power-law recession behavior through randomization of the response time. Depending on how response times are distribute, different recession forms emerge, however the power spectra of these functions preserves the $1/f^2$ scaling of the underlying linear reservoirs.

Distribution	$p_k(k)$	$q_N(t)$	Range in α
Uniform	$1/A$, $0 < k \leqslant A$	$\frac{q_o(1-e^{-At})}{At}$	−1 to −2
Exponential	$A\exp(-A\,k)$, $0 < A$	$\frac{Aq_o}{(A+t)}$	−1 to −2
Gamma	$\frac{k^{A-1}\exp(-Bk)B^A}{\Gamma(A)}, A, B > 0$	$q_o\left(\frac{B}{(B+t)}\right)^A$	−2
Single reservoir	1	$q_o\exp(-Ak)$, $0 < A$	0 to −2

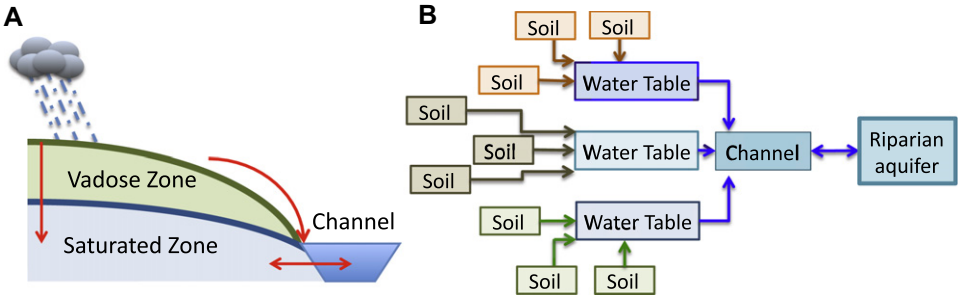

Fig. 5. Conceptual sketch indicating potential mechanisms of streamflow generation and their plausible arrangements in a primitive network. By recursively convolving the incoming flux with the reservoir linear response function, and then applying a combined distribution approach across each suite of parallel reservoirs, a response function for the network may be generated.

$$|Q(f)_N|^2 = \prod_{j=1}^{n} q_{oj}^2 \prod_{j=1}^{n} \frac{1}{\left(k_j^2 + f^2\right)}. \tag{32}$$

This expression can be simplified via a log transformation:

$$\begin{aligned}\log\left(|Q(f)_N|^2\right) &= \log\left(\prod_{j=1}^{n} q_{oj}^2\right) + \log\left(\prod_{j=1}^{n} \frac{1}{\left(k_j^2 + f^2\right)}\right) \\ &= 2\sum_{j=1}^{n} \log(q_{oj}) - \sum_{j=1}^{n} \log\left(k_j^2 + f^2\right) \\ &= 2n\overline{\log(q_o)} - n\overline{\log(k^2 + f^2)},\end{aligned} \tag{33}$$

where the overline indicates the expectation of the expression. From inspection, then, the form of the power spectrum is related to the geometric mean of the inflow and the time constants for the individual reservoirs, but cannot be further generalized without specifying $p_k(k)$. Comparing the empirical power spectra with the spectra in Eq. (32), suggests that it is again unnecessary to consider $n > 3$. For $n = 3$, the power spectrum is given by:

$$|Q(f)_3|^2 = q_{o1}^2 q_{o2}^2 q_{o3}^2 \frac{1}{\left(k_1^2 + f^2\right)\left(k_2^2 + f^2\right)\left(k_3^2 + f^2\right)}. \tag{34}$$

This spectrum evidently has a multi-scaling nature, spanning regimes that scale as $1/f^2$, $1/f^4$ and $1/f^6$ as f increases. If the three reservoirs are assumed to correspond to the vadose zone, the shallow water table and the channel, then k_1, k_2 and k_3 can be estimated, and the spectrum computed. Taking the response timescales as $O(10^{-1})$ (vadose zone), $O(10^{-2})$ (shallow water table) and $O(10^{-1})$ (channel) generates the spectrum shown in Fig. 6. As illustrated in Fig. 6, truncation of the spectrum at different frequencies generates the full range of α observed in real rivers. Such truncations arise with a fixed sampling frequency if the values of k_1–k_3 vary. If larger basins have smaller values of k (i.e. respond more gradually to a rainfall burst than small basins), then streamflow power spectra would be translated to lower frequencies with increasing drainage area. Daily sampling would truncate less of the multi-scaling region, leading to an increase in estimated α with drainage area.

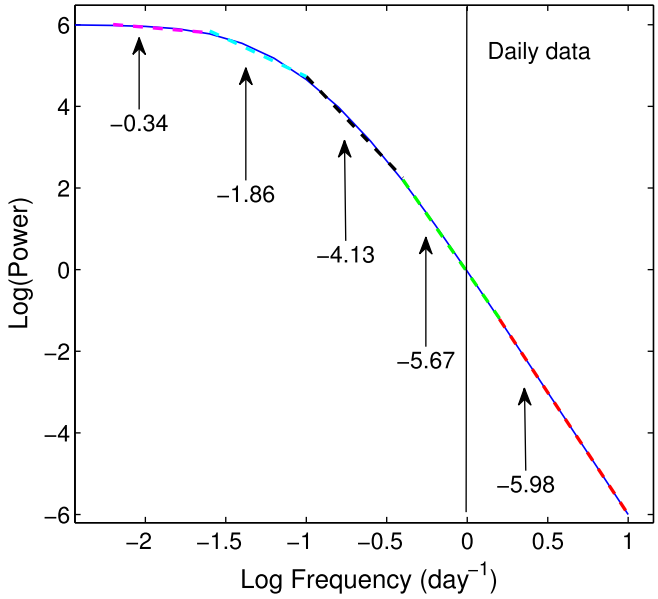

Fig. 6. Power spectrum generated from three reservoirs in series with different response times chosen to reflect reasonable orders of magnitude for soils, saturated zones and channels. The different regions indicate the best linear fit to the spectrum if it is truncated at progressively lower frequencies.

2.5. Idealized networks

Based on these results, attenuation of the flow signal and a reddening of the spectrum are associated with passage of the flow through new kinds of reservoirs, while passage through reservoirs in parallel alters the discharge hydrograph but not the scaling of the streamflow power spectrum. Together, these results suggest that the power spectrum of flow generated from a network in which individual flow paths consist of n reservoirs will have the same canonical form as the spectrum from n reservoirs in series. The nature of the flow at any level i in the network can be computed by determining the flow leaving an individual reservoir at that level, and then randomizing the relevant time constants. If the probability law for the time constants for every level i of the network is unaltered, then the flow leaving level i can be calculated as:

$$q_{out}^i(t) = \int_0^\infty p_k(k)\left[\int_0^t q_{in}^i(\tau) k_j \exp(-k_j(t-\tau))\mathrm{d}\tau\right]\mathrm{d}k. \tag{35}$$

In general, it is not possible to compute these flow responses analytically, but the effects of the transformations can be explored numerically. The predicted flow output at each scale preserves the signature of the series convolution, and is unaltered by the presence of parallel network branches, which the shifts in the spectrum along the network primarily attributable to the rising limb of the hydrograph.

2.6. Comparison with field data

The theoretical analysis suggests that the representation of a catchment as a third-order network of linear reservoirs is consistent with the form of empirical streamflow power spectra regardless of the heterogeneity in the properties of these reservoirs. If this mechanism is appropriate, then there should be empirical evidence of progressive reddening of incoming rainfall signatures as recorded in different 'reservoirs'.

Katul et al. [26] demonstrated that the measured soil moisture spectrum had a Lorentzian form with a high frequency scaling of $1/f^{\zeta+2}$, (where ζ is the exponent of the rainfall timeseries), which was strongly supported by high frequency soil moisture measurements made in the Duke Forest. Heuristically, if the flow leaving the vadose zone is primarily associated with gravitational drainage near saturation, then, following Clapp and Hornberger [41]:

$$q_{drainage} \propto K(\theta) \propto \theta^b. \tag{36}$$

That is, the spectrum of the flow leaving the vadose zone should reflect a power transformation of the soil moisture content. As discussed earlier, such a transformation does not alter the power spectrum of the soil moisture, suggesting that the flow leaving the vadose zone may also scale as $1/f^2$. Applying the stochastic soil moisture balance of Laio et al. [42], we find that the estimated deep drainage in that framework also scales as $1/f^2$ when driven by white noise. The vadose zone therefore appears to redden the rainfall signal.

Schilling and Zhang [43] studied the spectral properties of fluctuations in the water table from riparian transects at Walnut Creek (Iowa). Water table fluctuations 40 m from the stream had an average exponent (in the hourly to daily timescale range) of −2.38, while wells 20 m from the stream had an average exponent of −2.55, and wells 1 m from the stream had exponents of −3.4. The rainfall power spectrum scaled with an exponent of 0.04 in the same temporal range, while the power spectrum of the streamflow scaled as $1/f^{3.7}$.

The increase in α towards the channel suggests that a second reservoir, in addition to the vadose zone, is attenuating the rainfall signature. Two mechanistic interpretations are consistent with the spatial pattern in α. One interpretation is that as the upslope

contributing area increases towards the channel, the water table fluctuations are proportionally more influenced by lateral contributions from upslope. Because lateral contributions have been attenuated by storage and discharge from the hillslope aquifer, they contribute to a reddening of the spectrum of water table fluctuations compared to locations where the water table is primarily responding to local drainage from the vadose zone.

However, Walnut Creek is known to have substantial periods of reverse flow from the creek into the riparian aquifer [43]. Such reverse flow provides an alternative hypothesis for the observed trend in α: that the primary communication between the hillslope aquifer and the channel occurs due to rapid transmission of a pressure signal (which would preserve the $1/f^2$ scaling from the vadose zone), and that the channel network acts as a second reservoir. The similarity in exponents observed in the near-channel riparian aquifer and in the stream flow would then reflect the importance of the stream in controlling water fluctuations in the riparian zone, while attenuation of fluxes within the hillslope aquifers would have little if any effect on the high-frequency scaling of streamflow.

3. Discussion and Conclusions

3.1. Mechanisms for generating power-laws in streamflow

As illustrated in Fig. 1, power-laws are observed at multiple timescales in the streamflow spectra. In the hydrologic regime (daily - monthly timescales), power-law scaling arises under certain conditions. Firstly, the sampling frequency at which streamflow is measured must be sufficiently high compared to the limits of the power-law scaling regime that scaling exponents can be identified. This condition is met in the data from large basins presented here, but is not always met in very small basins where hourly sampling may be needed to resolve the high frequency regime. Secondly, the analyses here considered only basins where the assumption that flow generation can be approximated as the relaxation response to persistent rainfall shocks is reasonable. This means that arid basins where long periods of flow are dominated by baseflow, and cold basins, where large snowmelt pulses provide an additional signal of variation, have been neglected. As illustrated in Figs. 1 and 3, the dynamics discussed apply only on daily to monthly timescales. At higher frequencies, signatures associated with diurnal fluctuations in *et* or the turbulent characteristics of the streamflow may emerge, changing the scaling behavior. At lower frequencies, seasonal variation and long-period groundwater fluctuations perturb the discharge signal. Nonetheless, provided these caveats are met, power-law scaling of discharge timeseries on daily-monthly scales appears to be a general feature of streamflow.

Numerous potential sources of power-law scaling in streamflow have been reviewed and compared with observed features of the spectrum. Of the deterministic explanations reviewed, the classical linear-systems approach predicted power spectra that were most consistent with observations. Water balance and power law recession arguments confined scaling exponents to the $0 < \alpha < 2$ range, which is too restrictive compared to observations. Although hydraulic arguments allow for a range of spectral exponents, their predictions are quantitatively inconsistent with observations, or at least with the observations of individual flood events that can be reliably isolated from a streamflow timeseries.

3.2. Implications

Surprisingly the power spectra predicted from a simple linear conceptualization of catchment response were nearly identical to spectra predicted from the outflow of a nonlinear network with distributed parameters. On this basis, it also seems likely that the form of observed spectra would be insensitive to spatial variations in rainfall throughout a catchment, provided the rainfall scaling remained unaltered or remained 'white'. This may be plausible if the catchments primarily experienced one mode of rainfall – for instance frontal systems tend to have exponents near -0.5, while convective systems have exponents near -1 [44]. The results suggest that the observed range of spectral exponents ($0.5 \leqslant \alpha \leqslant 4.5$) in streamflow can be explained by several factors. Firstly, truncation associated with daily sampling reduces the empirical estimates of α from the theoretical maxima of $2n$. For instance, that the highest value of α reported elsewhere in the literature, 3.75, is based on hourly data that reduces this truncation effect [43]. Truncation may also explain the general trend of increasing observations of α with scale within individual basins: if the effective values of k_j increase with scale, then daily sampling truncates less of the high frequency scaling regime, leading to higher empirical estimates of α. Mixing of fluxes with different scaling may also alter the scaling regime. The scaling of numerically computed spectra at high frequencies is sensitive to fairly small injections of white-noise (e.g. contributing $\leqslant$5% of the variance in the streamflow), as might be associated with rainfall entering the channel directly. The preponderance of exponents in the range of $3 \leqslant \alpha \leqslant 4$ suggests that a 2-reservoir conceptualization may be the appropriate model for most of the watersheds investigated here. This would suggest that the vadose zone and the channel form the primary reservoirs for the rapid runoff response, and that the saturated zone does not greatly affect the high frequency scaling of streamflow.

Power-law scaling is an almost ubiquitous phenomenon across the earth, social, environmental, and life sciences, arising in fields as diverse as linguistics, demography or stratigraphy. One reason for its ubiquity is the broad range of fundamental processes that can promote power-law scaling [45]: combinations of exponentially distributed processes, critical phenomena, "rich-get-richer" mechanisms (the Yule phenomenon), reciprocal relationships with time in ODEs, and more [46]. Based on this review, the direct interpretation of power spectra in terms of underlying streamflow generation processes may prove challenging, since multiple combinations of flow pathways and network structures appear to preserve the overall structure of the streamflow spectrum. While it is theoretically possible to extract information about the response times of linear approximations to the different reservoirs in the system from the spectrum, fitting Eq. (34) to noisy data is likely to render these estimates uncertain. Although the link between the streamflow spectrum and the hydrograph remains robust, the convergence of multiple processes to a common set of streamflow power spectra poses a significant challenge to the mechanistic interpretation of hydrographs and streamflow spectral scaling.

Acknowledgements

The authors acknowledge support from the NSF through EAR – 1013339, AGS-110227, CBET-103347, the US Department of Agriculture (2011-67003-30222) and the Fulbright Italy distinguished scholars program.

References

[1] Sawicz K, Wagener T, Sivapalan M, Troch PA, Carrillo G. Catchment classification: empirical analysis of hydrologic similarity based on catchment function in the eastern USA. Hydrol Earth Syst Sci 2011;15:2895–911. doi:10.5194/hess-15-2895-2011.

[2] Brutsaert W, Nieber JL. Regionalized drought flow hydrographs from a mature glaciated plateau. Water Resour Res 1977;13(3):637–44. doi:10.1029/WR013i003p00637.

[3] Palmroth S, Katul G, Hui D, McCarthy H, Jackson R, Oren R. Estimation of long-term basin-scale evapotranspiration from streamflow time series. Water Resour Res 2010;46(W10512). doi:10.1029/2009WR008838.

[4] Kirchner JW. Catchments as simple dynamical systems: catchment characterization, rainfall-runoff modeling, and doing hydrology backward. Water Resour Res 2009;45(W02429). doi:10.1029/2008WR006912.
[5] Harman C, Sivapalan M. Effects of hydraulic conductivity variability on hillslope-scale shallow subsurface flow response and storage-discharge relations. Water Resour Res 2009;45(W01421). doi:10.1029/2008WR007228.
[6] Harman CJ, Sivapalan M, Kumar P. Power law catchment-scale recessions arising from heterogeneous linear small-scale dynamics. Water Resour Res 2009;45(W09404). doi:10.1029/2008WR007392.
[7] Troch PA, Detroch FP, Brutsaert W. Effective water-table depth to describe initial conditions prior to storm rainfall in humid regions. Water Resour Res 1993;29(2):427–34. doi:10.1029/92WR02087.
[8] Zhang Y, Schilling K. Temporal scaling of hydraulic head and river base flow and its implication for groundwater recharge. Water Resour Res 2004;40(3). doi:10.1029/2003WR002094.
[9] Zhang YK, Schilling K. Temporal variations and scaling of streamflow and baseflow and their nitrate-nitrogen concentrations and loads. Adv Water Resour 2005;28(7):701–10. doi:10.1016/j.advwatres.2004.12.014.
[10] Tallaksen LM. A review of baseflow recession analysis. J Hydrol 1995;165(1-4):349–70. doi:10.1016/0022-1694(94)02540-R.
[11] Botter G, Peratoner F, Porporato A, Rodriguez-Iturbe I, Rinaldo A. Signatures of large-scale soil moisture dynamics on streamflow statistics across us climate regimes. Water Resour Res 2007;43(11). doi:10.1029/2007WR006162.
[12] Botter G, Porporato A, Daly E, Rodriguez-Iturbe I, Rinaldo A. Probabilistic characterization of base flows in river basins: roles of soil, vegetation, and geomorphology. Water Resour Res 2007;43(6). doi:10.1029/2006WR005397.
[13] Pelletier JD, Turcotte DL. Long-range persistence in climatological and hydrological time series: analysis, modeling and application to drought hazard assessment. J Hydrol 1997;203(1-4):198–208. doi:10.1016/S0022-1694(97)00102-9.
[14] Pandey G, Lovejoy S, Schertzer D. Multifractal analysis of daily river flows including extremes for basins of five to two million square kilometres, one day to 75 years. J Hydrol 1998;208(1-2):62–81. doi:10.1016/S0022-1694(98)00148-6.
[15] Koscielny-Bunde E, Kantelhardt JW, Braun P, Bunde A, Havlin S. Long-term persistence and multifractality of river runoff records: detrended fluctuation studies. J Hydrol 2006;322(1–4):120–37. doi:10.1016/j.jhydrol.2005.03.004.
[16] Milly PCD, Wetherald RT. Macroscale water fluxes – 3. Effects of land processes on variability of monthly river discharge. Water Resour Res 2002;38(11). doi:10.1029/2001WR000761.
[17] Dolgonosov BM, Korchagin KA, Kirpichnikova NV. Modeling of annual oscillations and 1/f-noise of daily river discharges. J Hydrol 2008;357(3–4):174–87. doi:10.1016/j.jhydrol.2008.04.023.
[18] Clark C. Storage and the unit hydrograph. Trans Am Soc Civil Eng 1945;110:1419–46.
[19] Chapman T, Maxwell A. Baseflow separation – comparison of numerical methods with tracer experiments. In: Hydrology and water resources symposium. Hobart, Tasmania: Institute of Engineers Australia; 1996.
[20] Chapman T. A comparison of algorithms for stream flow recession and baseflow separation. Hydrol Process 1999;13(5):701–14.
[21] Huyck A, Pauwels V, Verhoest N. A base flow separation algorithm based on the linearized boussinesq equation for complex hillslopes. Water Resour Res 2005;41(W08415). doi:10.1029/2004WR003789.
[22] Troch P, Martinez G, Pauwels V, Durcik M, Sivapalan M, Harman C, et al. Climate and vegetation water use efficiency at catchment scales. Hydrol Process 2009;23(16):2409–14. doi:10.1002/hyp.7358.
[23] Fraedrich K, Larnder C. Scaling regimes of composite rainfall time series. Tellus, Ser A 1993;45:289–98.
[24] Botter G, Bertuzzo E, Rinaldo A. Transport in the hydrologic response: travel time distributions, soil moisture dynamics, and the old water paradox. Water Resour Res 2010;46(W03514). doi:10.1029/2009WR008371.
[25] Buttle J. Isotope hydrograph separations and rapid delivery of pre-event water from drainage basins. Progress Phys Geog 1994;18(1):16–41. doi:10.1177/030913339401800102.
[26] Katul GG, Porporato A, Daly E, Oishi AC, Kim HS, Stoy PC, et al. On the spectrum of soil moisture from hourly to interannual scales. Water Resour Res 2007;43(W05428). doi:10.1029/2006WR005356.
[27] Novick K, Stoy PC, Katul GG, Ellsworth DS, Siqueira MBS, Juang J, et al. Carbon dioxide and water vapor exchange in a warm temperate grassland. Oecologia 2004;138:259–74. doi:10.1007/s00442-003-1388-z.
[28] Stoy PC, Katul GG, Siqueira M, Juang JY, Novick K, McCarthy H, et al. Separating the effects of climate and vegetation on evapotranspiration along a successional chronosequence in the southeastern us. Global Change Biol 2006;12:1–21. doi:10.111/j.1365-2486.2006.01244.x.
[29] Botter G, Porporato A, Rodriguez-Iturbe I, Rinaldo A. Nonlinear storage-discharge relations and catchment streamflow regimes. Water Resour Res 2009;45(W10427). doi:10.1029/2008WR007658.
[30] Ceola S, Botter G, Bertuzzo E, Porporato A, Rodriguez-Iturbe I, Rinaldo A. Comparative study of ecohydrological streamflow probability distributions. Water Resour Res 2010;46(W09502). doi:10.1029/2010WR009102.
[31] Biswal B, Marani M. Geomorphological origin of recession curves. Geophys Res Lett 2010;37(L24403). doi:10.1029/2010GL045415.
[32] Higham D. An algorithmic introduction to numerical simulation of stochastic differential equations. Soc Ind Appl Math 2001;43(3):525–46.
[33] Van Atta C, Wyngaard J. On higher-order spectra of turbulence. J Fluid Mech 1975;72(4):673–94. doi:10.1017/S0022112075003229.
[34] Katul G, Parlange M, Albertson J, Chu CR. The random sweeping decorrelation hypothesis in stratified turbulent flows. Fluid Dynam Res 1995;16:275–95. doi:10.1016/0169-5983(95)00011-2.
[35] Rupp D, Selker J. On the use of the Boussinesq equation for interpreting recession hydrographs from sloping aquifers. Water Resour Res 2006;42(W12421). doi:10.1029/3006WR005080.
[36] Dooge J. A general theory of the unit hydrograph. J Geophys Res 1959;64(2):241–56. doi:10.1029/JZ064i002p00241.
[37] Nash JE. The form of the instantaneous unit hydrograph. Int Assoc Sci Hydrol 1957;45(3):114–21.
[38] Bras R, Rodriguez-Iturbe I. Random functions in hydrology. New York: Cambridge University Press; 1985.
[39] Beck C, Cohen E. Superstatistics. Physica A 2003;322:267–75. doi:10.1016/S0378-4371(03)00019-0.
[40] Sornette D. Critical phenomena in natural sciences. 2nd ed. New York: Springer; 2004.
[41] Clapp R, Hornberger G. Empirical equations for some soil hydraulic properties. Water Resour Res 1978;14(4):601–4. doi:10.1029/WR014i004p00601.
[42] Laio F, Porporato A, Ridolfi L, Rodriguez-Iturbe I. Plants in water-controlled ecosystems: active role in hydrologic processes and response to water stress – II. Probabilistic soil moisture dynamics. Adv Water Resour 2001;24:707–23. doi:10.1016/S0309-1708(01)00005-7.
[43] Schilling K, Zhang YK. Temporal scaling of groundwater level fluctuations near a stream. Groundwater; in press. doi:10.1111/j.1745-6584.2011.00804.x.
[44] Molini A, Katul G, Porporato A. Revisiting rainfall clustering and intermittency across different climatic regimes. Water Resour Res 2009;45(W11403). doi:10.1029/2008WR007352.
[45] Newman M. Power laws, Pareto distributions and Zipf's law. Contemp Phys 2006;46:323–51. doi:10.1080/00107510500052444.
[46] Montroll E, Schlesinger M. On 1/f noise and other distributions with long tails. Proc Natl Acad Sci USA 1982;79(2):3380–3.
[47] Tessier Y, Lovejoy S, Hubert P, Schertzer D, Pecknold S. Multifractal analysis and modeling of rainfall and river flows and scaling, causal transfer functions. J Geophys Res-Atm 1996;101(D21):26427–40. doi:10.1029/96JD01799.